A new concept of Compton Scattering tomography and the development of the corresponding circular Radon transform

Cécilia Tarpau, Javier Cebeiro, Marcela A. Morvidone and Maï K. Nguyen, *Senior Member, IEEE*

***Abstract*—A new modality of Compton Scattering Tomography is presented. This model is composed of a fixed source and detectors placed on a fixed ring passing through the source. This new modality, called Circular Compton Scattering Tomography, allows to register a complete set of data and, regarding constructive features like compactness or the absence of moving components, outperforms other existing Compton scattering tomography designs. A bi-imaging system combining this new system and Fan-beam computed tomography can also be considered, and such system will provide both the attenuation map and the distribution on electrons of the object under study. The modeling of the Circular Compton Scattering Tomography leads to the Radon transform on circles passing through a fixed point. A reconstruction algorithm based on an exact inversion formula of the Radon transform on circles is proposed and numerical simulations for image formation and reconstruction are carried out. The results show the viability of this new image system which is particularly suitable for small objects such as biomedical objects.**

***Index Terms*—Bi-imaging, Compton Scattering Tomography, Image formation, Image reconstruction, Radon Transform on circles**

I. Introduction

THE Radon transform (RT) established by Radon [1] in 1917 and the equivalent inverse formula found by Cormack [2], [3], [4] are the seminal works which allow the development of current Computed Tomography (CT). Conventional CT is based on the transmission of X-rays in matter and the transmitted flux density recovered by detectors. Thus, CT allows us to recover the attenuation map of an object.

CT uses only primary (not deviated) radiation to reconstruct the attenuation map of the object. However, there exists several ray-matter interactions which can deviate photons and Compton scattering is the dominant effect in the energy range of X and gamma rays used in medical applications [5] . Compton scattering causes blurring, loss of contrast in reconstructed images and may cause false detection. This is why conventional CT attempts to eliminate scattered radiation by the use of collimators.

C. Tarpau is with the ETIS (Equipes de Traitement de l'Information et Systèmes, University of Cergy-Pontoise / ENSEA / CNRS UMR 8051, 2, rue A. Chauvin, 95302 Cergy-Pontoise, France), the LPTM (Laboratoire de Physique Théorique et Modélisation, University of Cergy-Pontoise / CNRS UMR 8089, 2, rue A. Chauvin, 95302 Cergy-Pontoise, France) and the LMV (Laboratoire de Mathématiques de Versailles / CNRS UMR 8100, University of Versailles Saint Quentin, 45 avenue des Etats-Unis, 78035 Versailles, France) laboratories. E-mail: cecilia.tarpau@ensea.fr;

J. Cebeiro is with CEDEMA (Centro de Matemática Aplicada, Universidad Nacional de San Martín, Avenida 25 de Mayo y Francia, San Martín, Buenos Aires, Argentina) . E-mail: jcebeiro@unsam.edu.ar.

M. A. Morvidone is with CEDEMA (Centro de Matemática Aplicada, Universidad Nacional de San Martín, Avenida 25 de Mayo y Francia, San Martín, Buenos Aires, Argentina). E-mail: mmorvidone@unsam.edu.ar.

M. K. Nguyen is with the ETIS laboratory (Equipes de Traitement de l'Information et Systèmes, University of Cergy-Pontoise / ENSEA / CNRS UMR 8051, 2, rue A. Chauvin, 95302 Cergy-Pontoise, France). E-mail: mai.nguyen-verger@u-cergy.fr.

Manuscript received February, 12th 2018; revised ... .

A. Compton Scattering

When a source emits rays, part of these rays are scattered.

According to the Compton formula, the energy registered by a detector $E(\omega)$ is related to a scattering angle ω by

$$E(\omega) = \frac{E_0}{1 + \frac{E_0}{m\,c^2}\,(1 - \cos(\omega))}, \tag{1}$$

where E_0 is the energy of an emitted ray, $m\,c^2$ the energy of the electron at rest and $E(\omega)$ is the energy of the photon after interaction.

Towards the end of the past century, the idea of using the scattered radiation as a source of information came up, with the proposition of Compton Scattering Imaging (CSI) [6], [7] modalities. The idea behind Compton Scattering Imaging is to register scattered photons of given energy to reconstruct the object.

CSI systems have been proposed based on emission or transmission. Emission modalities have been proposed in [8], [9] and these modalities lead to V-line Radon transform for two-dimensional systems and conical Radon transforms for the three-dimensional ones. We will here focus on the second type of CSI which concerns transmission imaging, usually named Compton Scattering Tomography (CST). The functioning principle of such systems will be developed in the next paragraphs. The introduction of a combined modality with an emission / transmission imaging system has been also proposed in [10].

B. Compton Scattering Tomography (CST): functioning principle, advantages, challenges and short review

In a CST modality, the point source S emits primary radiation towards an object, of which M (scattering site) is a running point. A point detector D collects, at given energy $E(\omega)$, scattered radiation from the object.

The physics of Compton Scattering demands that the registered radiation flux at site D is due to the contribution of all scattering sites (electrons) M lying on an arc of circle from S

This article has been accepted for publication in a future issue of this journal, but has not been fully edited. Content may change prior to final publication. Citation information: DOI 10.1109/TRPMS.2019.2943555, IEEE Transactions on Radiation and Plasma Medical Sciences

to D subtending an angle $(\pi - \omega)$, where ω is the scattering angle corresponding to the outgoing energy $E(\omega)$, as given by (1) (see Fig. 1).

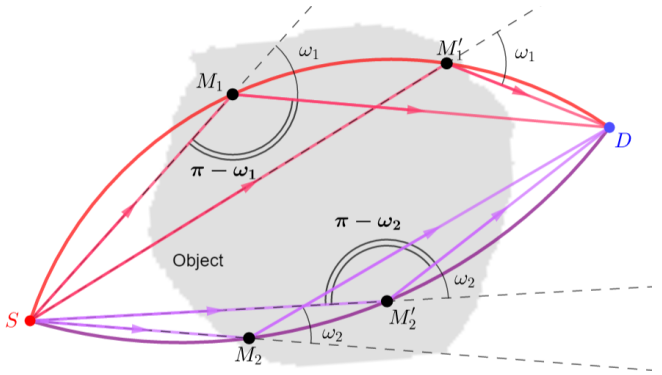

Fig. 1: Functioning principle of CST modalities

Consequently, CST is a new challenging technique which can offer the possibility to access a new type of information, which is the electronic density of the object, complementary to the attenuation map obtained by conventional CT.

Furthermore, CST has multiple advantages for biomedical imaging:

- the access to a directly measured electron density can be useful for radiation therapy applications [11]
- the higher contrast of scattering-based images compared to CT images, which would be helpful in imaging, for example, calcification in the breast or when scanning small objects (without an additional radiation dose) or in tracking tumors [11], [12].

However, CST modalities present a double challenge, both mathematical and technological. In fact, the modelling of integral data acquisition leads to generalizations of Radon transforms on families of circular arcs (CARTs). Consequently, the image reconstruction depends on the invertible corresponding CART.

Moreover, CST systems require multi-energy detectors with sufficient energy resolution. It is a challenge for detector technology.

Before introducing our new CST modality, we will give a short review of two previous main modalities in the next paragraphs.

1) First CST modality (proposed by S. J. Norton 1994): In the Norton's scanner [13], the source S is fixed and the detector D moves along a line intersecting the source site. Equivalently, a fixed array of detectors D_k, $k \in \{1, ..., K\}$ can be used (see Fig. 2).

Norton provided an inversion formula for his family of half of circles. A second inversion algorithm has been also proposed in [14], [15], based on the seminal work of Cormack on circles intersecting a fixed point. Then, an extended version of Norton's system has been studied [16] for one side scanning in large objects (in non-destructive evaluation, for example).

2) Second CST modality (proposed by Nguyen and Truong 2010): The model is composed of a source S, placed at a distance $2p$ from a detector D. The segment SD rotates around its middle point O and its angular position is given by the angle φ (see Fig. 3).

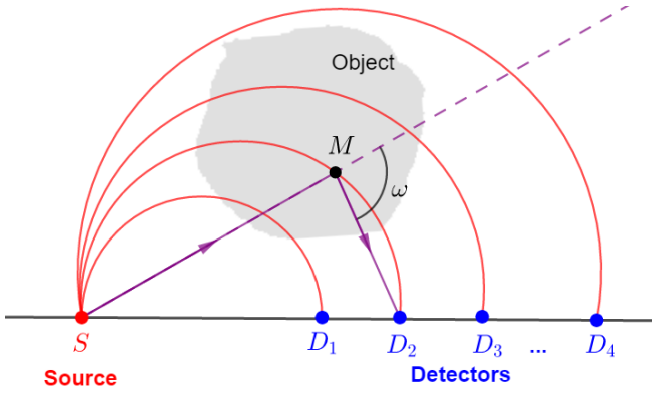

Fig. 2: Norton's modality (1994)

This modality is suitable for small objects scanning thanks to the rotation of the system around the object which can be placed inside the circle of centre O and of radius p.

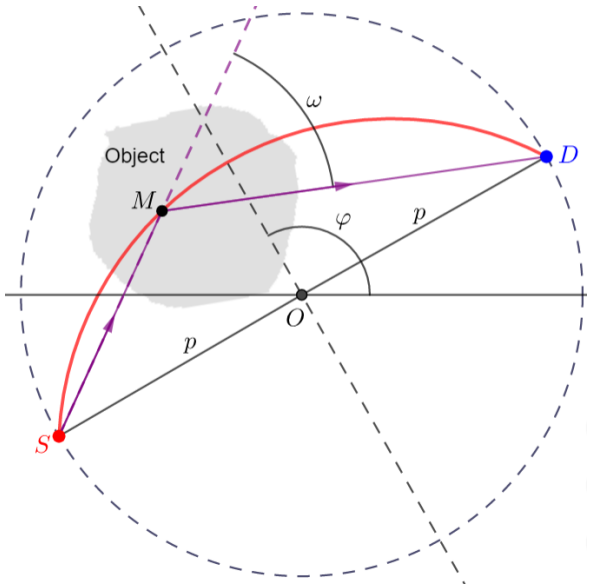

Fig. 3: Nguyen and Truong's modality (2010)

For a fixed position of the source S and the detector D, all photons scattered by the object and registered with the same energy by the detector have their scattering sites on a same circular arc passing through S and D.

Thus, this modality leads to a new generalized Radon transform on a family of circular arcs which has been inverted in [17], and the feasibility of this system has been proved with simulation results in [14], [15], [18].

C. Objectives of the paper

The aim of this paper is to propose a new CST which is completely fixed (fixed source and fixed detectors), while allowing to scan small objects. This modality allows to avoid motion of detectors (required for Nguyen's system) while having a compact system as those used in biomedical imaging.

The paper is organized as follows : section II introduces the new concept of CCST with its advantages and assumptions. The modelling of the CCST is presented in section III and the simulation in section IV. Open issues related to the general CST concept and particular CCST are discussed in section V. Concluding remarks end the paper.

II. New CST modality : Circular Compton Scattering Tomography (CCST)

A. Presentation of CCST

The proposed modality is composed of a source S and K fixed detectors D_k, $k \in \{1, ..., K\}$ placed on a ring passing through the source (see Fig. 4). This modality is named Circular Compton Scattering Tomography (CCST).

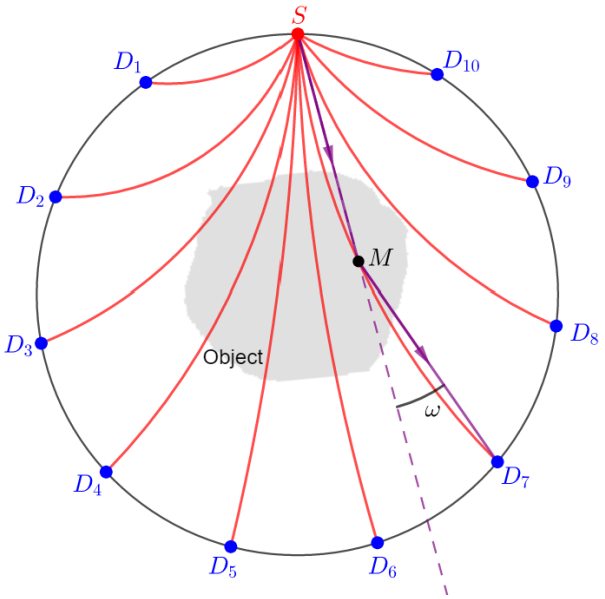

Fig. 4: Circular Compton Scattering Tomography modality

B. Main advantages of CCST

The new modality of CST has the following features and some advantages regarding previous modalities:

1) No motion or rotation of Source - Detector couple is needed to obtain a complete dataset for image reconstruction.
2) Geometry of CCST is convenient for small object scanning.
3) The detector ring (multiple detectors) of CCST allows to reduce the practical scanning time and thus the time of exposure to radiation. In addition, the circular layout of detectors reduces the size of the system in comparison with the linear configuration.
4) Possibility of combining CCST with conventional fan-beam CT to design a double imaging system thanks to the similar configuration of two systems (see Fig. 5). In fact, if the detectors of the system are set to register the primary photon energy (E_0), the system works as fan-beam CT. Nevertheless, this complementary configuration requires mechanical rotation of the system to have a complete dataset. When the detectors register the energies lower than E_0, the system operates as CCST. Then, this bi-imaging system provides both the attenuation map (by fan-beam CT) and the distribution of electrons (by CCST), which are two physical properties of the object under study.

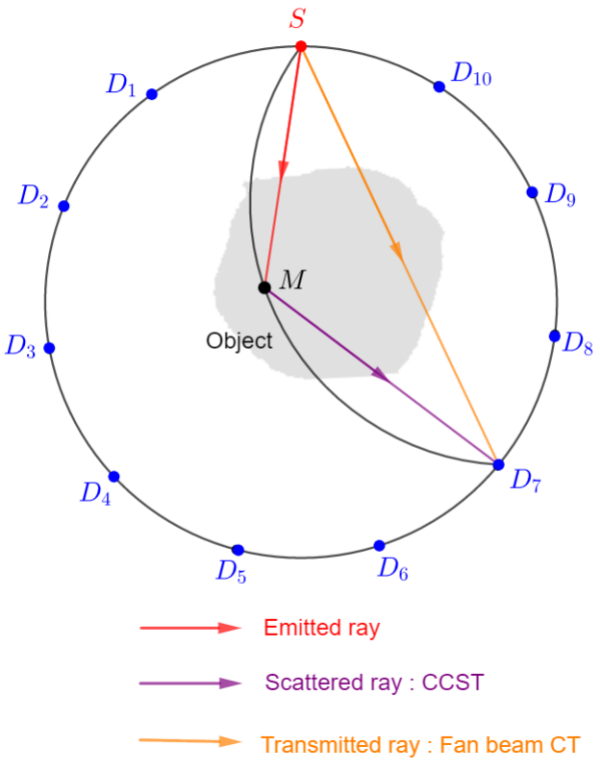

Fig. 5: Bi-imaging system combining Fan-beam CT and CCST

C. General assumptions for the study of the modelling of CCST

All scattered photons collected by a detector D_k at the same energy arise from scattering sites lying on a circular arc with S and D_k as extremities subtending a angle $(\pi - \omega)$. In this work, we take into account the circles which are supporting the considered scanning circular arcs, with the understanding that the external part (outside of the detector ring) of the circles give no contribution in data acquisition.

Consequently, the scattered radiation flux density registered by detectors can be modelled by a generalized Radon transform on circles passing through a fixed point.

However, the analysis described here and in many other publications of CST ([13], [16], [17], [19], [20], [21]) is idealized. In fact, for the sake of mathematical tractability, it is assumed that :

- first order scattering is so dominant that the higher order scattering can be neglected,
- attenuation is absent,
- we have idealized detectors with perfect energy resolution.

These assumptions provide insight into the reconstruction problem in the same way that the inverse classical Radon

This article has been accepted for publication in a future issue of this journal, but has not been fully edited. Content may change prior to final publication. Citation information: DOI 10.1109/TRPMS.2019.2943555, IEEE Transactions on Radiation and Plasma Medical Sciences

transform does as the idealized solution to the conventional CT problem. Furthermore, additional issues such as detector performance or accounting for attenuation are discussed in section V.

III. Modelling of the new modality of CCST

A. Setup of the system

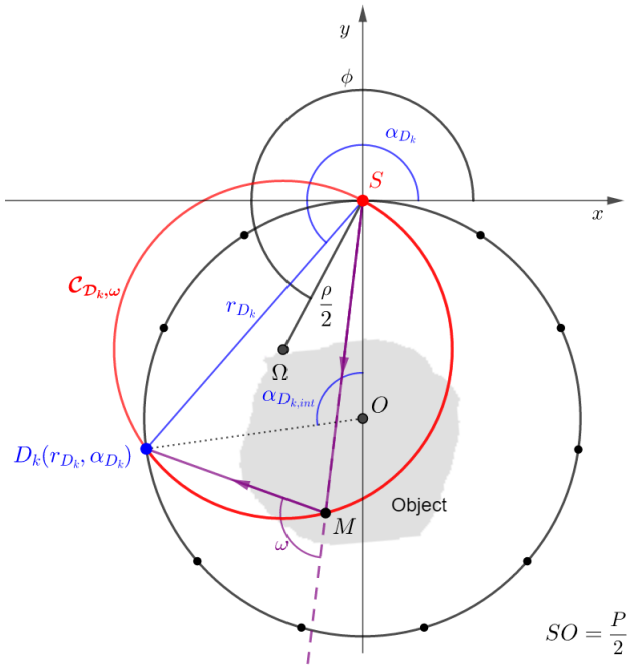

Fig. 6: Principle of our CCST - In black: fixed ring of detectors, in red: example of scanning circle

We consider a non-moving source S at the origin of our coordinates system and a fixed ring of K detectors D_k with $k \in \{1, 2, ..., K\}$ passing through the source (see Fig. 6). Denoting P as the diameter of the fixed ring of detectors, the polar equation of the ring centered at O is

$$r = P \cdot \cos\left(\alpha + \frac{\pi}{2}\right), \alpha \in [\pi, 2\pi[. \tag{2}$$

In order to have a constant distance between adjacent detectors, we define first $\alpha_{D_{k_int}}$ the angle subtending the y-axis and the radius OD_k of the fixed ring (see Fig. 6):

$$\alpha_{D_{k,int}} = 2\pi \frac{k}{K+1}. \tag{3}$$

Angle $\alpha_{D_{k_int}}$ is related to polar angular coordinate α_{D_k} of detector D_k according to the relation

$$\alpha_{D_k} = \pi + \frac{\alpha_{D_{k,int}}}{2}. \tag{4}$$

With (3) and (4), one can make explicit polar coordinates (r_{D_k}, α_{D_k}) of each detector D_k :

$$D_k(r_{D_k}, \alpha_{D_k}) \text{ with } \begin{cases} r_{D_k} & = P\cos\left(\alpha_{D_k} + \frac{\pi}{2}\right) \\ \alpha_{D_k} & = \pi\left(1 + \frac{k}{K+1}\right). \end{cases} \tag{5}$$

Elementary geometry allows to verify that the distance d between adjacent detectors is uniform:

$$d = ||D_{k+1}D_k|| = P\sin\left(\frac{\pi}{K+1}\right) = \text{constant}. \tag{6}$$

B. Parametrization of the scanning circles

In the rest of the paper, the parameters (r, θ) denote the polar coordinates of a point on a circle. First of all, the family of the scanning circles passing through the origin has the following general equation form, depending on its diameter ρ and its angle ϕ relative to x-axis

$$C_{D_k,\omega}(\rho, \phi) : r = \rho(D_k, \omega) \cdot \cos\left(\theta - \phi(D_k, \omega)\right), \quad \theta \in [\pi, 2\pi[. \tag{7}$$

An example of such scanning circle, centered at Ω, is shown with a particular scattering site denoted M in Fig. 6.

The parameters of each scanning circle depend on the considered detector D_k and the scattering angle ω as follows:

$$\begin{cases} \rho\left(D_k, \omega\right) & = r_{D_k} / \sin\left(\omega\right) \\ \phi\left(D_k, \omega\right) & = \alpha_{D_k} + \omega - \frac{\pi}{2} \end{cases} \tag{8}$$

where $\omega \in]0, \pi[$.

C. Image acquisition

Data measurement for this system is modelled by the integral of the electronic density on the parametric circles. This integral is called the Radon transform on circles passing through a fixed point (CirRT):

$$\mathcal{R}_{\text{Cir}} f(\rho, \phi) = \int_{\mathcal{C}_{D_k,\omega}(\rho,\phi)} f(r, \theta) ds \tag{9}$$

where ds is the integration element on the circle $\mathcal{C}_{D_k,\omega}(\rho, \phi)$. Equation (9) is the image formation equation.

Moreover, it can be written with a delta function kernel as follows :

$$\mathcal{R}_{\text{Cir}} f(\rho, \phi) = \int_0^{\infty} dr \int_{\pi}^{2\pi} d\theta\, \rho f(r, \theta) \delta(r - \rho\cos\left(\theta - \phi\right)). \tag{10}$$

This formulation (10) shows that the presence of noise or missing data may cause important instabilities in image reconstruction.

D. Image reconstruction

In a previous work, Cormack [4] defined two families of curves and established the equations of the forward and inverse Radon transforms for these families. Our family of circles is a special case of his curves.

Using *consistency conditions* [3], he proposed a stable solution for the inverse transform for its family of parametrized curves. Then, we rewrite the Cormack reconstruction equation in our case, as follows :

This article has been accepted for publication in a future issue of this journal, but has not been fully edited. Content may change prior to final publication. Citation information: DOI 10.1109/TRPMS.2019.2943555, IEEE Transactions on Radiation and Plasma Medical Sciences

$$f(r,\theta) = \mathcal{R}_{\text{Cir}}^{-1} f(r,\theta) = \frac{1}{2\pi^2 r} \int_0^{2\pi} d\phi \quad \text{p.v.} \left\{ \int_0^{\infty} d\rho \frac{\partial \mathcal{R}_{\text{Cir}} f(\rho,\phi)}{\partial \rho} \frac{\rho}{r - \rho\cos(\theta-\phi)} \right\} \quad (11)$$

where $p.v.$ denotes Cauchy principal value.

Equation (11) is the image reconstruction equation.

In order to numerically implement (11), we use the Hilbert transform, denoted $\mathcal{H}$ and defined as follows:

$$\mathcal{H}\{u\}(t) = \frac{1}{\pi} \text{ p.v.} \left\{ \int_{-\infty}^{\infty} \frac{u(\tau)}{t-\tau} d\tau \right\} \quad (12)$$

Then, (11) becomes:

$$f(r,\theta) = \mathcal{R}_{\text{Cir}}^{-1} f(r,\theta) = \frac{1}{2\pi r} \int_0^{2\pi} d\phi \; \frac{1}{cos(\theta-\phi)} \mathcal{H}\left\{ \frac{\partial \mathcal{R}_{\text{Cir}} f(\rho,\phi)}{\partial \rho} \cdot \rho \right\} \left(\frac{r}{\cos(\theta-\phi)} \right). \quad (13)$$

In (13), the Hilbert transform can be easily computed via the Fourier transform.

IV. Simulation of the new modality and results

The simulations were carried out using for a medical object, the Shepp-Logan phantom (see Fig. 7).

A. Parameter choices

The size of the object is $N \times N = 512 \times 512$ pixels.

The phantom is placed inside a ring of detectors of radius proportional to the size of the object, that is 512 length unities. We place on the circular ring a detector per unit length, what represents an amount of $N_D = 3712$ detectors. For the number of projections, we take $N_\omega = N_\phi = 3000$.

These parameter choices satisfy the condition $N_\phi \times N_D > N \times N$ [22], which gives the lower limitation for data acquisition with uniform sampling and in the absence of perturbations such as noise or missing data. In our case, N_D and N_ϕ were overestimated because of the spatial non uniform sampling with acquisition on circles.

B. Image formation

We first simulate the acquisition of physical data using parameters $\alpha_{D_{k,int}}$, which gives us the angular position of the considered detector D_k on the fixed ring, and ϕ, which is related to the scattering angle ω according to (8).

Given a detector D_k and a scattering angle ω, we denote Ω the center of the corresponding circle $\mathcal{C}_{D_k,\omega}$. Cartesian coordinates of Ω are

$$\begin{cases} x_\Omega &= \frac{\rho(D_k,\omega)}{2} \left(\cos\left(\phi(D_k,\omega)\right)\right) \\ y_\Omega &= \frac{\rho(D_k,\omega)}{2} \left(\sin\left(\phi(D_k,\omega)\right)\right). \end{cases} \quad (14)$$

Then, a point M with the Cartesian coordinates (x,y) belongs to the circle $\mathcal{C}_{D_k,\omega}$, centered at Ω if

$$(x(\gamma), y(\gamma)) = (x_\Omega, y_\Omega) + \frac{\rho(D_k,\omega)}{2}(\cos\gamma, \sin\gamma), \quad \gamma \in [0, 2\pi[\quad (15)$$

Hence, we obtain the following parametrization for scanning circles

$$\mathcal{C}_{D_k,\omega} : \begin{cases} x(\gamma) &= \frac{\rho(D_k,\omega)}{2} \left(\cos(\gamma) + \cos\left(\phi(D_k,\omega)\right)\right) \\ y(\gamma) &= \frac{\rho(D_k,\omega)}{2} \left(\sin(\gamma) + \sin\left(\phi(D_k,\omega)\right)\right), \end{cases} \quad \gamma \in [0, 2\pi[\quad (16)$$

We finally obtain the forward transform formula for implementation

$$\mathcal{R}_{\text{Cir}} f(\alpha_{D_{k,int}}, \phi) = \frac{\rho}{2} \int_0^{2\pi} f\left(x(\gamma), y(\gamma)\right) d\gamma \quad (17)$$

Figure 8 shows the result of data acquisition.

This result cannot be used directly: in fact, to reconstruct our object, the data acquisition have to be relative to the parameters (ρ, ϕ) according to (9). This change of variables is carried out by data interpolation and the result is showed on Fig. 9. Data acquisition has the form of the letter U with a slight hole on his basis (see Fig. 9): this hole is due to the missing detectors near to the source and is filled with a spline interpolation.

C. Image reconstruction

1) Formulation: We proceed similarly to transform (13) in Cartesian coordinates. With

$$\begin{cases} r &= \sqrt{x^2+y^2} \\ r\cos(\theta-\phi) &= x\cos\phi + y\sin\phi, \end{cases} \quad (18)$$

Equation (13) becomes

$$f(x,y) = \mathcal{R}_{\text{Cir}}^{-1} f(x,y) = \frac{1}{2\pi} \int_0^{2\pi} d\phi \; \frac{1}{x\cos\phi + y\sin\phi} \mathcal{H}\left\{ \frac{\partial \mathcal{R}_{\text{Cir}} f(\rho,\phi)}{\partial \rho} \cdot \rho \right\} \left(\frac{x^2+y^2}{x\cos\phi + y\sin\phi} \right). \quad (19)$$

Furthermore, for the simulations, we will compute the Hilbert transform in the Fourier domain. In fact, we have

$$\mathcal{H}\{u\}(t) = \mathcal{F}^{-1}(-i \cdot \text{sign}(\nu) \cdot \mathcal{F}(u)(\nu))(t). \quad (20)$$

where $\mathcal{F}$ denotes the 1D Fourier transform.

Finally, the image reconstruction equation used for simulation is

$$f(x,y) = \mathcal{R}_{\text{Cir}}^{-1} f(x,y) = \frac{1}{2\pi} \int_0^{2\pi} d\phi \; \frac{1}{x\cos\phi + y\sin\phi} \cdot \mathcal{F}^{-1}\left(-i \cdot \text{sign}(\nu) \mathcal{F}\left(\frac{\partial \mathcal{R}_{Cir} f(\rho,\phi)}{\partial \rho} \rho \right)(\nu) \right) \left(\frac{x^2+y^2}{x\cos\phi + y\sin\phi} \right) \quad (21)$$

This article has been accepted for publication in a future issue of this journal, but has not been fully edited. Content may change prior to final publication. Citation information: DOI 10.1109/TRPMS.2019.2943555, IEEE Transactions on Radiation and Plasma Medical Sciences

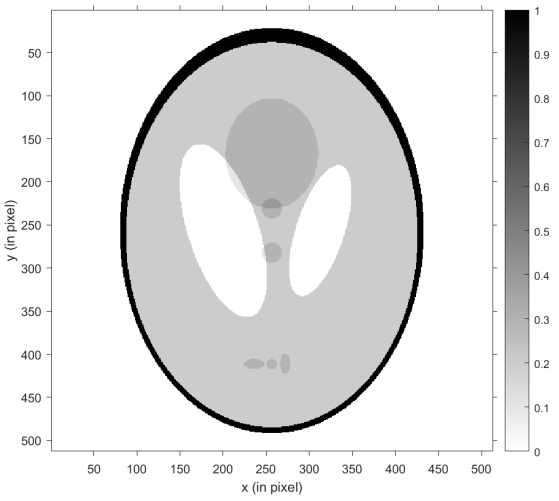

Fig. 7: Original object : Shepp-Logan phantom

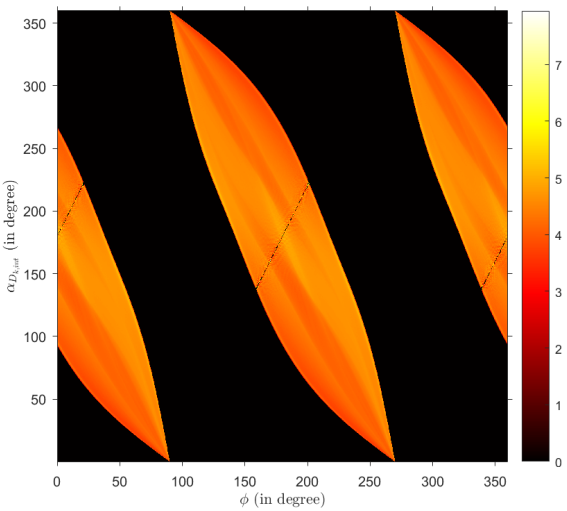

Fig. 8: Image formation $\mathcal{R}_{\text{Cir}}f(\alpha_{D_{k,int}}, \phi)$ of the original object in Fig.7 (in a logarithmic scale)

2) General reconstruction algorithm: Considering (21), the general algorithm for image reconstruction is as follows:

1) Compute the discrete derivation of the projections and multiply the result by ρ,
2) Apply the filter associated to Hilbert tranform (20) in Fourier domain
3) For each ϕ, interpolate the data on the considered circles,
4) Weight the result with factor $1/(x\cos\phi + y\sin\phi)$,
5) Sum the weighted interpolations on all directions ϕ,
6) Normalize by $1/2\pi$.

To our knowledge, it is the first time that the reconstruction equation (21) has been numerically implemented.

In order to evaluate the quality of the reconstructions, we use the Normalized Mean Square Error (NMSE) defined by

$$\text{NMSE} = \frac{\sum_{(i,j)\in[|1,N|]^2} (I_o(i,j) - I_r(i,j))^2}{\max_{(i,j)\in[|1,N|]^2} I_o(i,j)^2} \cdot \frac{1}{N^2} \qquad (22)$$

where I_o and I_r are respectively the original and the reconstructed images.

3) Result of image reconstruction and remarks: Figure 10 shows the result of reconstruction for the Sheep-Logan phantom.

It is noted that the image is well recovered in the whole. In fact, the little nodules at the middle and at the bottom of the reconstruction are well visible. This result shows the feasibility of this modality for the requirements of biomedical imaging.

However, we observe some artifacts on the left and right sides of the object which are less well reconstructed than the up and bottom of the object. These artifacts will be explained in the next section.

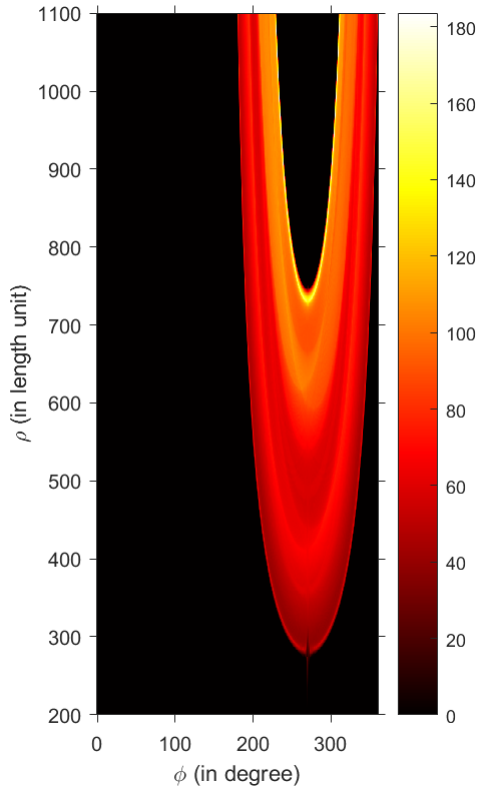

Fig. 9: Rearranged $\mathcal{R}_{\text{Cir}}f(\rho, \phi)$ of acquired data in Fig.8

D. Artifact characterization

Reconstructions exhibit some artifacts that are due to missing data, see for example the lower left and right edges of the phantom in Fig. 10. In CCST, the lack of data is an intrinsic problem since projections are limited to circles with a finite diameter, i.e. radius ρ labelling data is constrained to a range $(0, \rho_{\max})$.

Such artifacts consist of singularities that can be explained via microlocal analysis. In the case of the Radon transform on straight lines studied by Nosmas [23], Quinto, Frikel and Krishnan [24], [25], [26] microlocal analysis allowed artifact characterization and image enhancement. These articles considered cases where missing data was deliberately chosen to mimic a real limitation in the scanning. Some properties

This article has been accepted for publication in a future issue of this journal, but has not been fully edited. Content may change prior to final publication. Citation information: DOI 10.1109/TRPMS.2019.2943555, IEEE Transactions on Radiation and Plasma Medical Sciences

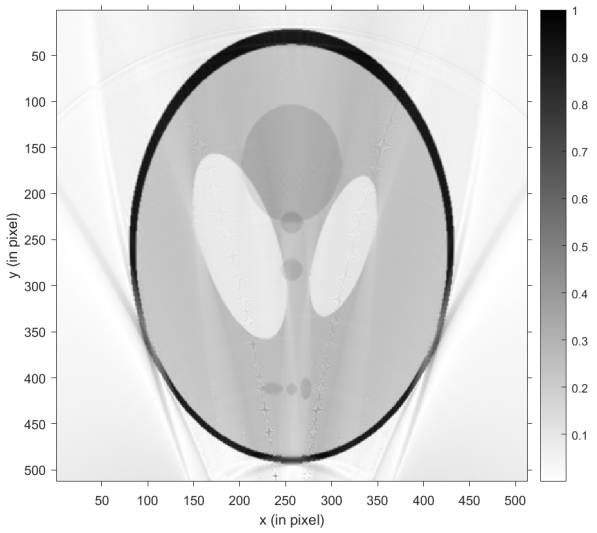

Fig. 10: Image reconstruction - NMSE = 0.0063

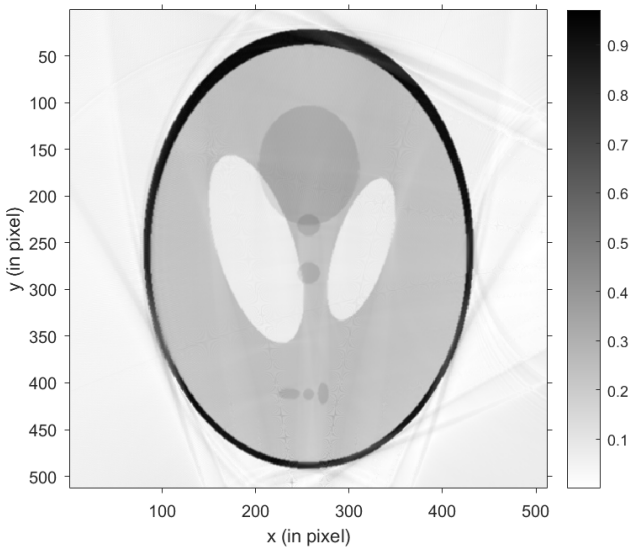

Fig. 11: Image reconstruction with two data acquisitions - NMSE = 0.0068

established by Frikel and Quinto can be extrapolated to our generalized Radon transform. It can be proven that the CirRT is an Integral Fourier Operator (IFO), like the classical Radon transform. In fact, considering the integral definition of Dirac function,

$$\delta(s) = \frac{1}{2\pi}\int_{-\infty}^{+\infty} e^{i\xi s} d\xi, \tag{23}$$

the CirRT can be rewritten as

$$\mathcal{R}_{Cir} f(\rho,\phi) = \int_{R^2\times[0,2\pi]} \frac{\rho}{2\pi r} f(r,\theta) e^{i\xi(\rho - r\cos(\theta-\phi))} r\, d\xi\, dr\, d\theta. \tag{24}$$

Thus, this formulation shows that the CirRT is an IFO with phase function $\Phi(\xi) = \xi(r - \rho\cos(\theta-\phi))$ and amplitude $\frac{\rho}{2\pi r}$. Then, provided that CirRT in an IFO, we can extend the results established for IFO's in literature in the form of a principle predicting reconstruction quality:

The boundary of an object is visible if there exists a scanning circle with is locally tangent to this boundary. If any scanning curve is not tangent to a local part of the boundary, this local part of the boundary is considered as invisible, and will not be well reconstructed.

According to this, the lower reconstruction quality in the lower edges of the object in Fig. 10 is a consequence of the lack of scanning circles locally tangent to these parts. In order to illustrate that, we show the effect of a second data acquisition with the new source position shifted $\pi/2$ from the first one. The result is an improved image quality because the second scanning compensates the lack of information in the first one. Figure 11 shows the result obtained after the combination of the two data acquisitions. Although NMSE does not changes significantly, image quality is clearly improved since left and right edges are better reconstructed and artifacts inside the object are also reduced.

V. Open issues and perspectives

This first work on this new modality opens some new perspectives of different kind which will be explored in future works.

A. Taking into account scattering and attenuation

Taking into account attenuation either for CCST or for other CST modalities is a major challenge that so far has not exact solution.

In transmission CST, the attenuation affects both scattered and primary photons but in a different way. Mathematically, the attenuation is modelled by two factors a_1 for emitted ray and a_2 for scattered ray:

$$a_1(E_0, SM) = \exp\left(-\int_{SM} \mu(E_0, M)\, dl(M)\right) \tag{25}$$

$$a_2(E(\omega), MD) = \exp\left(-\int_{MD} \mu(E(\omega), M)\, dl(M)\right) \tag{26}$$

where μ is the attenuation coefficient which depends on the energy (E_0 for primary photons or $E(\omega)$ for the energy of scattered photons) and on the propagation distance (SM or MD). This fact leads to an attenuated Radon transform on circular arcs including a_1 and a_2 as follows:

$$g(SD,\omega) = K(\omega)\cdot \int_{M\in \text{Arc SD}} a_1(E_0, SM)\, f(M)\, a_2(E(\omega), MD)\, dl(M), \tag{27}$$

where $K(\omega)$ is the kinematic factor of Compton effect [15].

For the kind of (27) no exact solution is known until now.

However, iterative algorithms for correcting attenuation have been proposed which either correct the reconstructed function [27] with the generalized Chang Correction (GCC) or correct data acquisition [28] with the iterative pre correction (IPC). For the previous Nguyen and Truong's modality, the

problem has been addressed using an extended version of IPC algorithm [29]. This method requires having the operator T^{-1}, i.e. the inverse operator for the corresponding non attenuated Radon transform. This approach is also feasible for CCST, where the operator T^{-1} is the inverse Radon transform on circles $\mathcal{R}_{\text{Cir}}^{-1} f$. This is why establishing the inverse Radon transform for CST modalities is the first important step in order to have a complete modelling accounting for attenuation. A method similar to [29] will be studied for the CCST in a future work.

B. Technological challenges raised by CST modalities

CCST and more generally CST need multi-energy detectors with a sufficient resolution. The performance of detector has a great influence on the quality of reconstructed images. A study on the influence of energy resolution on image reconstruction quality were proposed in [30]. Another interesting extension of this work is to extend this study for the CCST modality using Monte-Carlo simulations in combination with anthropomorphic phantoms [31].

VI. Concluding remarks

Using wisely the information given by Compton scattered rays continues to be a relevant challenge today.

The new modality of Compton scattering tomography (CCST) presented here falls within this context with additional advantages comparative to the previous proposed modalities.

In fact, the CCST gathers the advantage to be a fixed system while collecting a complete dataset for image reconstruction and able to scan small objects. Moreover, thanks to the similarity between the CCST and the fan-beam CT configurations we can propose a bi-imaging system combining them to obtain two physical properties of matter : attenuation map and electronic density.

From a practical point of view, the multiple (ring) detectors allows to reduce the acquisition time and thus the radiation dose. In addition, the circular distribution of detectors reduces the size of the system.

From a mathematical point of view, the modelling of this new system leads to a generalized Radon transform on a family of circles passing through a fixed point. The equations of image formation and reconstruction have been explicitly formulated and the numerical algorithms were implemented for the first time. This work is the first important step before taking into account the practical aspects (attenuation, spatial and energy resolution, noise, ...).

Moreover, the quality of reconstruction is suitable for the requirements of biomedical imaging. This confirms the feasibility of this new CCST modality in the sense that the information contained in the measurements of scattered radiation is sufficient to recover the electronic density of an object.

VII. Funding and acknowlegdments

C. Tarpau research work is supported by grants from Région Ile-de-France (in Mathematics and Innovation) 2018-2021 and LabEx MME-DII (Modèles Mathématiques et Economiques de la Dynamique, de l'Incertitude et des Interactions) (No. ANR-11-LBX-0023-01).

J. Cebeiro and M. A. Morvidone are partially suported by SOARD-AFOSR (grant number FA9550-18-1-0523). J. Cebeiro research work is supported by a CONICET postdoctoral grant (Leg. 171800).

The authors would like to thank also the Institute for Advanced Studies (IAS) of the University of Cergy Pontoise in France for the financial support given to this research project.

References

[1] J. Radon, "Über die Bestimmung von Funktionen durch ihre Integralwerte längs gewisser Mannigfaltigkeiten," *Akad. Wiss.*, vol. 69, pp. 262–277, 1917.

[2] A. M. Cormack, "Representation of a function by its line integrals, with some radiological applications," *Journal of Applied Physics*, vol. 34, no. 9, pp. 2722–2727, 1963.

[3] ——, "Radons problem–old and new," in *SIAM-AMS Proceedings*, vol. 14. American Mathematical Society, 1984, pp. 33–39.

[4] ——, "The Radon transform on a family of curves in the plane," *Proceedings of the American Mathematical Society*, vol. 83, no. 2, pp. 325–330, 1981.

[5] F. M. Khan and J. P. Gibbons, *Khan's the physics of radiation therapy*. Lippincott Williams & Wilkins, 2014.

[6] S. Gautam, F. Hopkins, R. Klinksiek, and I. Morgan, "Compton interaction tomography I. Feasibility studies for applications in earthquake engineering," *IEEE Transactions on Nuclear Science*, vol. 30, no. 2, pp. 1680–1684, 1983.

[7] N. V. Arendtsz and E. M. Hussein, "Energy-spectral Compton scatter imaging. I. Theory and mathematics," *IEEE Transactions on Nuclear Science*, vol. 42, no. 6, pp. 2155–2165, 1995.

[8] M. K. Nguyen, T. T. Truong, M. Morvidone, and H. Zaidi, "Scattered radiation emission imaging: Principles and applications," *Journal of Biomedical Imaging*, vol. 2011, p. 13, 2011.

[9] M. K. Nguyen, T. T. Truong, C. Driol, and H. Zaidi, "On a novel approach to Compton scattered emission imaging," *IEEE Transactions on Nuclear Science*, vol. 56, no. 3, pp. 1430–1437, 2009.

[10] G. Rigaud, R. Régnier, M. K. Nguyen, and H. Zaidi, "Combined modalities of Compton scattering tomography," *IEEE Transactions on Nuclear Science*, vol. 60, no. 3, pp. 1570–1577, 2013.

[11] G. Redler, K. C. Jones, A. Templeton, D. Bernard, J. Turian, and J. C. Chu, "Compton scatter imaging: A promising modality for image guidance in lung stereotactic body radiation therapy," *Medical physics*, vol. 45, no. 3, pp. 1233–1240, 2018.

[12] K. C. Jones, G. Redler, A. Templeton, D. Bernard, J. V. Turian, and J. C. Chu, "Characterization of Compton-scatter imaging with an analytical simulation method," *Physics in Medicine & Biology*, vol. 63, no. 2, p. 025016, 2018.

[13] S. J. Norton, "Compton scattering tomography," *Journal of Applied Physics*, vol. 76, no. 4, pp. 2007–2015, 1994.

[14] G. Rigaud, M. K. Nguyen, and A. K. Louis, "Circular harmonic decomposition approach for numerical inversion of circular radon transforms," in *Proceedings of the 5th International ICST Conference on Performance Evaluation Methodologies and Tools*. ICST (Institute for Computer Sciences, Social-Informatics and Tools), 2011, pp. 582–591.

[15] ——, "Novel numerical inversions of two circular-arc Radon transforms in Compton scattering tomography," *Inverse Problems in Science and Engineering*, vol. 20, no. 6, pp. 809–839, 2012.

[16] J. Cebeiro, M. K. Nguyen, M. Morvidone, and A. Noumowé, "New improved Compton scatter tomography modality for investigative imaging of one-sided large objects," *Inverse Problems in Science and Engineering*, vol. 25, no. 11, pp. 1676–1696, 2017.

[17] M. K. Nguyen and T. T. Truong, "Inversion of a new circular-arc Radon transform for Compton scattering tomography," *Inverse Problems*, vol. 26, no. 6, p. 065005, 2010.

[18] G. Rigaud, M. K. Nguyen, and A. K. Louis, "Modeling and simulation results on a new Compton scattering tomography modality," *Simulation Modelling Practice and Theory*, vol. 33, pp. 28–44, 2013.

[19] J. Webber and E. T. Quinto, "Microlocal analysis of a compton tomography problem," *arXiv preprint arXiv:1902.09623*, 2019.

[20] T.-T. Truong and M. K. Nguyen, "Compton scatter tomography in annular domains," *Inverse Problems*, 2019.

[21] J. Webber, "X-ray compton scattering tomography," *Inverse problems in science and engineering*, vol. 24, no. 8, pp. 1323–1346, 2016.
[22] R. N. Bracewell, "Numerical transforms," *Science*, vol. 248, no. II May, pp. 697–704, 1990.
[23] J.-C. Nosmas, "Analyse Microlocale et Tomographie Géométrique," in *ICAOS'96*. Springer, 1996, pp. 338–344.
[24] J. Frikel and E. T. Quinto, "Artifacts in incomplete data tomography with applications to photoacoustic tomography and sonar," *SIAM Journal on Applied Mathematics*, vol. 75, no. 2, pp. 703–725, 2015.
[25] E. T. Quinto, "Artifacts and visible singularities in limited data X-ray tomography," *Sensing and Imaging*, vol. 18, no. 1, p. 9, 2017.
[26] V. P. Krishnan and E. T. Quinto, "Microlocal analysis in tomography," *Handbook of mathematical methods in imaging*, pp. 1–50, 2014.
[27] L.-T. Chang, "A method for attenuation correction in radionuclide computed tomography," *IEEE Transactions on Nuclear Science*, vol. 25, no. 1, pp. 638–643, 1978.
[28] A. Maze, R. Collorec, P. Bourguet, and M. Pierpittte, "Iterative reconstruction methods for non uniform attenuation distribution in spect," in *1992 14th Annual International Conference of the IEEE Engineering in Medicine and Biology Society*, vol. 5. IEEE, 1992, pp. 1821–1822.
[29] O. A. O. Guerrero, G. Rigaud, R. Régnier, and M. K. Nguyen, "Attenuation correction in a new modality of Compton Scattering Tomography," in *Interdisciplinary Symposium on Signal and Sytems for Medical Applications (ISSSMA'13)*, Paris, France, 2013.
[30] M. K. Nguyen, J.-L. Delarbre, and T. Truong, "Study of the influence of energy resolution on image reconstruction quality in emission imaging based on Compton scattered radiation," in *IEEE Nuclear Science Symposium-Medical Imaging Conference*, Dresden, Germany, 2008.
[31] W. Kainz, E. Neufeld, W. E. Bolch, C. G. Graff, C. H. Kim, N. Kuster, B. Lloyd, T. Morrison, P. Segars, Y. S. Yeom *et al.*, "Advances in Computational Human Phantoms and Their Applications in Biomedical Engineering A Topical Review," *IEEE Transactions on Radiation and Plasma Medical Sciences*, vol. 3, no. 1, pp. 1–23, 2019.